

Morphology and crystallization kinetics in HfO₂ thin films grown by atomic layer deposition

M.-Y. Ho and H. Gong^{a)}

Department of Materials Science, National University of Singapore, 119260, Singapore

G. D. Wilk, B. W. Busch,^{b)} and M. L. Green

Agere Systems, Electronic Device Research Laboratory, Murray Hill, New Jersey 07974

P. M. Voyles,^{c)} D. A. Muller, and M. Bude

Bell Laboratories, Lucent Technologies, 600 Mountain Avenue, Murray Hill, New Jersey 07974

W. H. Lin and A. See

Chartered Semiconductor Manufacturing Limited, Singapore 738406, Singapore

M. E. Loomans and S. K. Lahiri^{d)}

Institute of Materials Research and Engineering, Singapore 119260, Singapore

Petri I. Räisänen

ASM America Incorporated, 3440 East University Drive, Phoenix, Arizona 85034

(Received 28 May 2002; accepted 8 November 2002)

We report the effects of annealing on the morphology and crystallization kinetics for the high- κ gate dielectric replacement candidate hafnium oxide (HfO₂). HfO₂ films were grown by atomic layer deposition (ALD) on thermal and chemical SiO₂ underlayers. High-sensitivity x-ray diffractometry shows that the as-deposited ALD HfO₂ films on thermal oxide are polycrystalline, containing both monoclinic and either tetragonal or orthorhombic phases with an average grain size of ~ 8.0 nm. Transmission electron microscopy shows a columnar grain structure. The monoclinic phase predominates as the annealing temperature and time increase, with the grain size reaching ~ 11.0 nm after annealing at 900 °C for 24 h. The crystallized fraction of the film has a strong dependence on annealing temperature but not annealing time, indicating thermally activated grain growth. As-deposited ALD HfO₂ films on chemical oxide underlayers are amorphous, but show strong signatures of ordering at a subnanometer level in Z-contrast scanning transmission electron microscopy and fluctuation electron microscopy. These films show the same crystallization kinetics as the films on thermal oxide upon annealing. © 2003 American Institute of Physics.

[DOI: 10.1063/1.1534381]

INTRODUCTION

The search for suitable candidates to replace SiO₂ as the gate dielectric in future sub-100-nm complementary metal oxide semiconductor (CMOS) devices¹ has recently received enormous attention.² Of the many different materials with high dielectric constants κ , which have been used as SiO₂ replacements,² hafnium oxide (HfO₂) is one of the most promising. HfO₂ is compatible with polysilicon processing,^{2–6} has a high dielectric constant of $\kappa \sim 16–25$,^{2,7–9} and has demonstrated very encouraging initial device characteristics.^{10–15}

The thermal stability of high- κ materials in direct contact with Si and SiO₂ has also emerged as a key issue in selecting suitable high- κ candidates. The thermal stability of HfO₂ films in contact with Si and SiO₂ has been studied for HfO₂ deposited by atomic layer deposition (ALD),¹⁶ ion

beam assisted deposition,¹⁷ metalorganic chemical vapor deposition,¹⁸ and jet vapor deposition (JVD).¹²

The as-deposited structure of HfO₂ films is also at issue. Zhu *et al.*¹² report that as-deposited JVD HfO₂ does not show a clear crystalline peak in x-ray diffraction, indicating that the film is amorphous. Amorphous layers are generally preferred for gate oxides, but a polycrystalline layer may also be acceptable. Hergenrother *et al.*¹³ have demonstrated metal–oxide–semiconductor field-effect transistors using ALD HfO₂ and poly-Si gates with extremely low leakage current densities ($J_G \sim 10^{-7}$ A/cm² for an equivalent oxide thickness of ~ 15 Å), in which the HfO₂ gate oxide is polycrystalline. Using a polycrystalline gate dielectric film with a large grain size will help minimize the variations in the effective electric field experienced by the charge carriers in the channel. This suggests that a large, predictable grain size may be a useful selection criterion for high- κ candidate materials.

It is therefore important to understand the kinetics of crystallization of pure HfO₂ films when they are subjected to the high temperatures used in conventional CMOS processing, a subject that has received very little attention. We have

^{a)} Author to whom correspondence should be addressed; electronic mail: masgongh@nus.edu.sg

^{b)} Present address: Micron Technology, Boise, ID 83707.

^{c)} Present address: Department of Materials Science and Engineering, University of Wisconsin—Madison, Madison, WI 53706.

^{d)} Present address: NanoNexus Inc., Fremont, CA 94539.

studied the morphology and crystallization kinetics of HfO_2 films deposited by ALD on thermal and chemical SiO_2 layers on Si as a function of annealing time and temperature. ALD is the most reliable and manufacturable of the existing oxide deposition techniques. It produces uniform, high-quality films with excellent step coverage and controllable thickness down to a few Ångströms across 200 or 300 mm wafers.^{19–21} This level of uniformity is essential for future CMOS processing.

We have used high-sensitivity x-ray diffractometry and cross-sectional transmission electron microscopy (TEM) to characterize these films. X-ray diffraction (XRD) was performed using a two-dimensional (2D) angle-resolved detector, which greatly increases the sensitivity to small fractions of crystallized material or small grain sizes. We have also employed fluctuation electron microscopy,²² an electron diffraction technique, to measure the residual degree of order in the subset of as-deposited films that are amorphous.

EXPERIMENTAL PROCEDURE

HfO_2 films 20 nm thick were grown by ALD on *p*-Si(100) substrates ($\rho=5\text{--}10\ \Omega\text{cm}$). The detailed atomic layer deposition mechanism has been reported elsewhere.²³ Before deposition, substrates were treated with a diluted HF solution to remove the native oxides, followed by growth of either thermal or chemical oxide layers. The thermal oxides were 0.5 nm thick, and 0.55-nm-thick chemical oxides were formed by rinsing the HF-last wafers with deionized water that contains ~ 5 ppm O_3 . A thin interfacial SiO_2 layer greatly facilitates uniform film growth and is essential to ensuring a linear growth rate for HfO_2 in the ALD process. HfO_2 growth on H-terminated Si is very nonuniform.²⁴ An excess of each precursor was supplied alternately to saturate the surface sites and ensure self-limiting film growth. Excess species and gaseous by-products were purged with N_2 at a flow rate of ~ 800 sccm to prevent any gas phase reactions.²⁵ HfO_2 films were grown using alternating pulses of hafnium tetrachloride (HfCl_4) and H_2O , using N_2 as a carrier gas. The ALD process was performed in an ASM Pulsar 2000™ module at 300 °C and a chamber pressure of ~ 1.5 Torr. The anneals were performed in a tube furnace with an N_2 ambient at atmospheric pressure.

X-ray diffraction patterns were obtained using a Brücker-AXS system with a 2D angle-resolved area detector.²⁶ The unique feature of an area detector is the ability to simultaneously detect the diffracted beam intensities over a large range of χ and 2θ angles with little or no sample or detector movement. In a conventional XRD system, diffraction out of the diffractometer plane is not detected; thus, the materials structure represented by the missing diffraction data will either be ignored, or extra sample rotation is needed to complete the measurements. All samples were measured with the detector held fixed at $2\theta=45^\circ$. The samples were continuously rotated through the range of $10^\circ < 2\omega < 40^\circ$. Phase identification was done by integration over the range of $-65^\circ < \chi < -115^\circ$ along the Debye rings to yield peak intensity versus 2θ plots in a range of $15^\circ < 2\theta < 65^\circ$. All samples were measured with a 500 s exposure to ensure

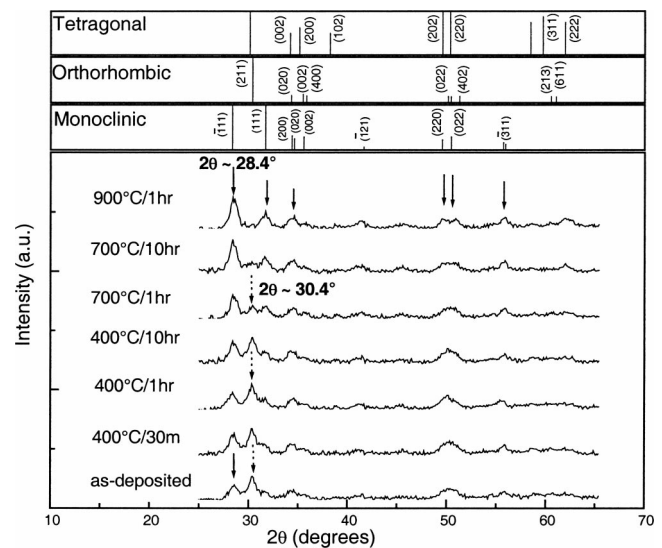


FIG. 1. XRD spectra of ALD HfO_2 films on a thermal oxide underlayer, showing the effect of annealing at for different times and different temperatures. The top panel shows the peak positions and intensities for three main crystalline phases of HfO_2 , obtained from powder diffraction ICDD card files. The decrease in intensity of the peak at $2\theta=30.4^\circ$ (dashed arrow) indicates the transformation of either the tetragonal or orthorhombic phase into the monoclinic phase ($2\theta=28.4^\circ$, solid arrow) as the annealing temperature and time increase. The transformation is complete after annealing at 700 °C for 10 h, shown by the absence of the peak at $2\theta=30.4^\circ$ in that spectrum.

comparable signal-to-noise ratios, and the Si background was subtracted from each spectrum. The crystallite size was inferred based on the Scherrer formula, $L = 0.94\lambda / W_{\text{eff}} \cos \theta$, where L is the structural coherence length, λ is the wavelength of the x-ray radiation (0.1542 nm), θ is the half angle of the scattering vector, and W_{eff} is the effective full width at half maximum (FWHM) of the x-ray peak, corrected for instrumental broadening by $W_{\text{eff}}^2 = W_{\text{meas}}^2 - W_{\text{system}}^2$.²⁷ We take $W_{\text{system}} = 0.527^\circ$, the measured FWHM of the (111) Si peak. We used a well-developed HfO_2 peak near $2\theta=28.4^\circ$ to estimate the grain size and the degree of crystallinity of the film. In this study, use of the phrase “degree of crystallinity” refers to the fraction of crystallized material in an amorphous matrix.

Electron microscopy and electron diffraction experiments were performed in a JEOL 2010F ARP-STEM operated at 200 kV. Cross-section samples were prepared by tripod polishing and imaged in a $\langle 110 \rangle$ orientation. Fluctuation electron microscopy experiments were performed using scanning transmission electron microscopy (STEM) microdiffraction²⁸ with a 5 Å FWHM electron probe.

RESULTS AND DISCUSSION

Figure 1 shows the XRD patterns for the HfO_2 films on thermal oxide after annealing at a series of different temperatures and times. The top panel shows the peak positions and intensities for crystalline HfO_2 from the powder diffraction ICDD card files. For all of the resolved peaks in the spectra (solid arrows) except one, the peak near $2\theta=30.4^\circ$ (dashed arrow) corresponds to the monoclinic crystal standard. The peak at 30.4° corresponds to either a tetragonal or ortho-

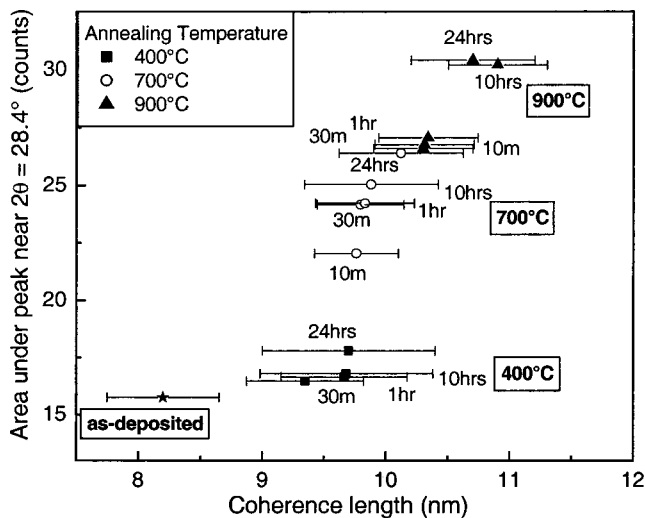


FIG. 2. Degree of crystallinity as a function of grain size showing thermally activated grain growth behavior during annealing. The FWHM and integrated area of the $(\bar{1}11)$ peak in the x-ray spectra are extracted from Gaussian fits to the peaks. The mean grain size is calculated from the FWHM using the Scherrer formula, assuming equiaxed grains. The area under the same peak is proportional to the fraction of the sample that has crystallized upon heat treatment. The error bars are derived from Gaussian fits.

rhombic phase. Both phases may be present, as the peaks could overlap in our XRD spectra; additional study is required to determine which phase is present. Our results are consistent with the results of Aarik *et al.*,²⁹ who observed an orthorhombic phase in ALD HfO_2 films grown at 500 °C. Ritala *et al.*³⁰ also observed weak peaks at the same position of $2\theta=30.4^\circ$. As annealing temperature and time are increased, all monoclinic peaks grow in intensity, while the peak near $2\theta=30.4^\circ$ does not, suggesting that the monoclinic phase is preferred during grain growth in furnace annealing. Additional data (not shown) acquired at a series of intermediate annealing temperatures and times between the values shown in Fig. 1 show the same trend.

The area detector images from which Fig. 1 is derived show continuous rings, indicating that the films on thermal oxide are polycrystalline with equiaxed grains. We can therefore measure the grain size and the degree of crystallinity of the film from the characteristics of the $(\bar{1}11)$ peak. The FWHM and area of the $(\bar{1}11)$ reflection ($2\theta=28.4^\circ$) were determined by fitting each spectrum to a Gaussian line shape. The area is related to the degree of crystallinity, and we deduce the structural coherence length (i.e., mean grain size) from the FWHM using the Scherrer formula as described above.

Figure 2 shows peak areas as a function of the grain size at various annealing temperatures and times, which illustrates the evolution of the ALD HfO_2 grain growth. The degree of crystallinity depends strongly on the annealing temperature but only weakly on annealing time. Only a very small change in grain size was observed even after a long anneal of 24 h (Fig. 2), indicating that grain growth in this system is thermally activated. There was no significant change in the integrated areas upon annealing at 900 °C for 24 h, suggesting that the films have fully crystallized.

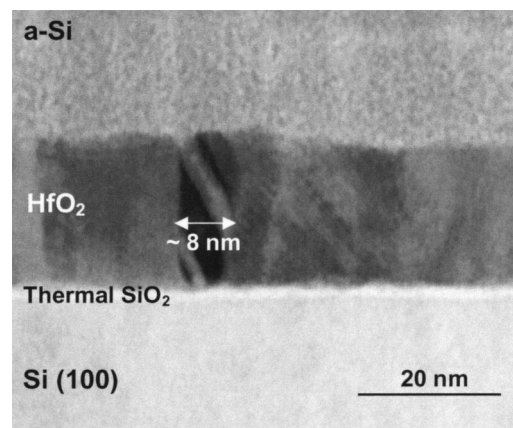


FIG. 3. Bright-field cross-sectional TEM image showing a large ~ 8 nm, columnar grain in the as-deposited ALD HfO_2 film grown on a thermal SiO_2 layer. The height of the grain spans the entire film thickness.

A typical microstructure for a 20 nm ALD HfO_2 film grown on a ~ 1 nm thermal SiO_2 layer is shown in the cross-sectional TEM of Fig. 3. The polycrystalline nature of the HfO_2 film on thermal SiO_2 is evident. The grain size as measured by TEM for the as-deposited films is in very good agreement with values calculated using the Scherrer formula, as described above. TEM also shows that the grain morphology is columnar, with the height of the grains approximately equal to the film thickness.

Films deposited on a chemically grown SiO_2 underlayer have a very different microstructure. Figure 4 is a high-resolution (HR) annular dark-field (ADF) “Z-contrast” STEM image of this sample. This imaging mode is particularly well-suited to characterization of thin oxide layers because it is incoherent.³¹ The Si lattice is visible across the bottom. The SiO_2 underlayer is the thin dark band just above the lattice. The image intensity in this mode scales as $Z^{1.7}$, where Z is the atomic number of the species under the beam, so the HfO_2 is the bright band across the top of the image.

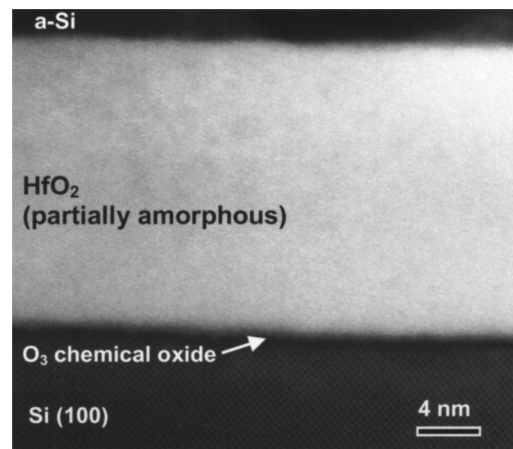


FIG. 4. ADF Z-contrast STEM image of a 20-nm-thick as-deposited ALD HfO_2 film on a chemical oxide underlayer. The Si lattice is visible across the bottom; above it is the SiO_2 underlayer, followed by the HfO_2 film. The HfO_2 is not crystalline, but if it were fully disordered, it would not show any contrast in this imaging mode. Instead, it shows some stipling, suggesting the presence of some sort of intermediate-range ordering in the structure.

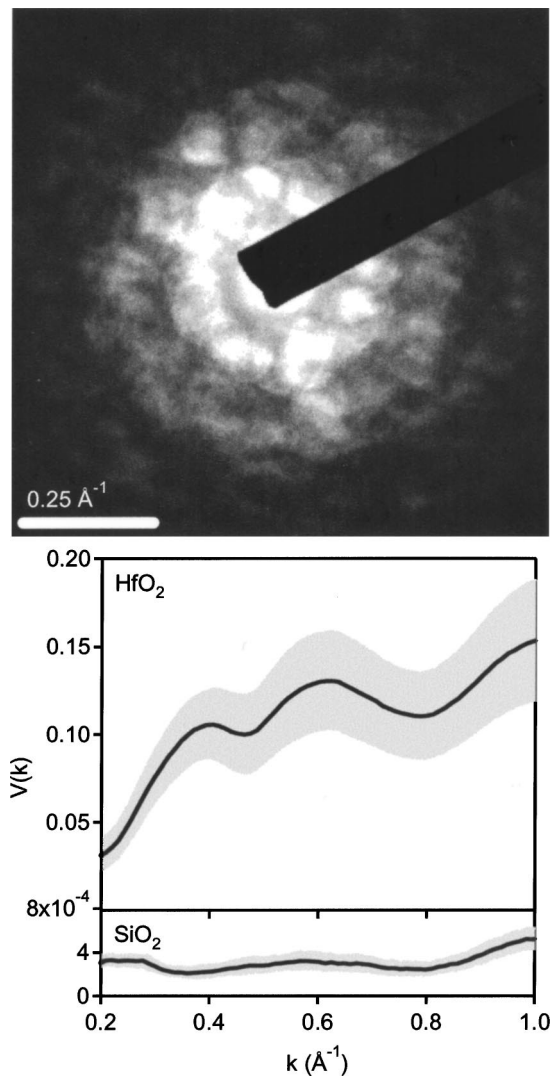


FIG. 5. (Top) convergent beam electron diffraction pattern from the HfO_2 on chemical oxide film, measured with a 5 \AA probe. A true glass such as SiO_2 would show undifferentiated diffuse rings. This sample shows crystal-like disks, but not in crystalline symmetry, again indicating intermediate range order. (Bottom) fluctuation electron microscopy $V(k)$ data for the same sample compared to a pure SiO_2 sample. $V(k)$ is much larger for the HfO_2 than for SiO_2 , showing conclusively that the HfO_2 is ordered.

The most striking and unusual feature of this image is that there is visible structure in the HfO_2 that is *not* a crystal lattice. There are no visible crystal grains in the film, which would suggest that it is amorphous. In ADF STEM, however, an amorphous material should show no contrast; the familiar speckle pattern from amorphous samples in high-resolution TEM (such as the *a*-Si layer at the top of Fig. 3) occurs because HRTEM is a coherent imaging mode. Without the coherence, there should be no contrast (see, for example, the images in Muller³¹ and Busch *et al.*³²). Figure 4, therefore, suggests that the ALD HfO_2 deposited on chemical oxide has less order than a crystal, but more order than a true glass such as SiO_2 . The top panel of Fig. 5 is a convergent beam electron diffraction (CBED) pattern from the same sample; the disk-like features are suggestive of the disks that would be observed from a crystal, but they are not fully formed and they do not exhibit crystalline symmetry.

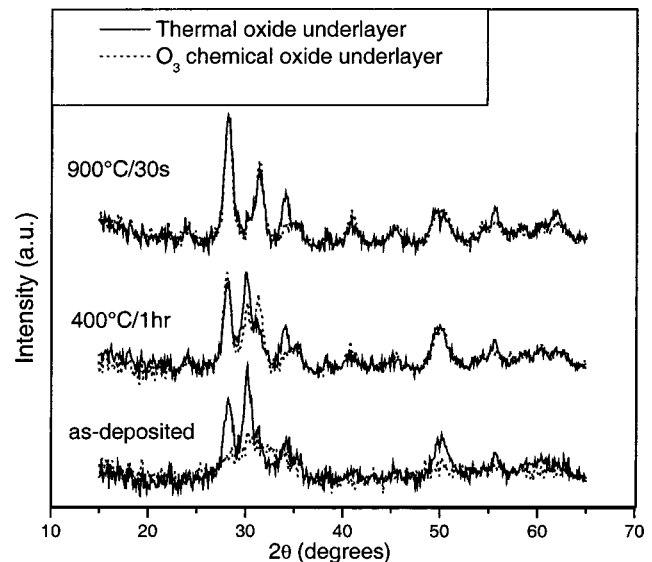


FIG. 6. 20 nm ALD HfO_2 films grown on a thermal oxide underlayer (solid line) and a chemical oxide underlayer (dotted line). Only extremely weak reflections were detected from the as-deposited film with a chemical oxide underlayer, suggesting that the films were either amorphous or nanocrystalline. Upon annealing, the peak intensities from both films achieve the same height and FWHM, indicating that there is no significant difference in the crystallization kinetics.

Fluctuation electron microscopy (FEM) is uniquely sensitive to this sort of intermediate-range order.²² In FEM, we measure diffraction from many small volumes of the sample, in the form of CBED patterns like those in Fig. 5.²⁸ If there are large fluctuations in the diffracted intensity from place to place, the structure is heterogeneous and ordered; if the fluctuations are small, the structure is homogeneous and disordered.²² We use the statistical variance V of the diffracted intensity distribution as a quantitative measure of the magnitude of the fluctuations.

The bottom panel of Fig. 5 shows V as a function of the scattering vector magnitude k for the HfO_2 film and, for comparison to a true glass, an SiO_2 film deposited by chemical vapor deposition. The magnitude of $V(k)$ for the HfO_2 film is two orders of magnitude larger than $V(k)$ for the SiO_2 film. $V(k)$ for the HfO_2 is, in fact, larger than that for any amorphous material ever measured, including amorphous silicon, germanium, and carbon. This indicates that this sample has a great deal of order at the 5 \AA length scale probed by these measurements. The form of this order is as yet undetermined, but it could be small ($\sim 1 \text{ nm}$ or less) crystal-like clusters. Competition between clusters of the monoclinic, orthorhombic, and tetragonal phases might prevent overall crystallization.

This result is further supported by the XRD spectrum of the HfO_2 on chemical oxide (dotted line), shown as a function of annealing temperature in Fig. 6. The as-deposited sample shows primarily the broad maxima characteristic of an amorphous sample, with a very weak peak near $2\theta = 30.4^\circ$. This may indicate a very small crystalline fraction in the orthorhombic or tetragonal phase; STEM and FEM investigate only a small region of the film and might miss a very low density of crystals. Thicker films are known to

facilitate crystal nucleation,³⁰ so it is not surprising to observe very fine-grain nanocrystallinity in a HfO₂ film only 20 nm thick.

Despite the difference in as-deposited structure, HfO₂ films deposited on both thermal and chemical SiO₂ underlayers exhibit similar crystallization kinetics, as shown in Fig. 6 by the fact that the peak intensity of both films increases up to the same height and FWHM on annealing. A similar observation has been made by Lysaght *et al.*,³³ in which 4 nm as-deposited ALD HfO₂ films grown on chemical oxide underlayers appear amorphous. Results in the same study³³ show that the percentage of the crystallinity achieved after annealing is independent of the as-deposited crystallinity.

CONCLUSIONS

As-deposited ALD HfO₂ films grown on thermal SiO₂ are polycrystalline, while the same films deposited on chemical SiO₂ are amorphous but strongly ordered on a subnanometer scale. The HfO₂ films deposited on chemical oxide may be very-fine-grain (~1 nm) nanocrystalline; further experiments are required to elucidate the structure. Subsequent heat treatments of both systems show very similar crystallization kinetics, resulting in grain growth to a relatively large grain size of about 10 nm, after even a short anneal at 900 °C.

ACKNOWLEDGMENTS

The authors wish to thank R. B. van Dover and T. Siegrist for useful discussions and technical assistance during the XRD measurements. The authors are also thankful to T. W. Sorsch for assistance in fabrication.

¹International Technology Roadmap for Semiconductors (Semiconductor Industry Association, San Jose, CA, 2001) [<http://public.itrs.net/>].

²G. D. Wilk, R. M. Wallace, and J. M. Anthony, *J. Appl. Phys.* **89**, 5243 (2001).

³B. H. Lee, R. Choi, L. Kang, S. Gopalan, R. Nieh, K. Onishi, Y. Jeon, W.-J. Qi, C.-S. Kang, and J. C. Lee, *Tech. Dig. Int. Electron Devices Meet.* **2000**, 39.

⁴B. H. Lee, L. Kang, W.-J. Qi, R. Nieh, Y. Jeon, K. Onishi, and J. C. Lee, *Tech. Dig. Int. Electron Devices Meet.* **1999**, 133.

⁵K. Onishi, C. S. Kang, R. Choi, H.-J. Cho, S. Gopalan, R. Nieh, E. Dharmarajan, and J. C. Lee, *Tech. Dig. Int. Electron Devices Meet.* **2001**, 659.

⁶Q. Lu, R. Lin, H. Takeuchi, T.-J. King, C. Hu, K. Onishi, R. Choi, C.-S. Kang, and J. C. Lee, *Proceedings of the 2001 International Semiconductor Device Research Symposium* (2001), p. 377.

⁷Y.-S. Lin, R. Puthenkovilakam, and J. P. Chang, *Appl. Phys. Lett.* **81**, 2041 (2002).

⁸B. H. Lee, L. Kang, R. Nieh, W.-J. Qi, and J. C. Lee, *Appl. Phys. Lett.* **76**, 1926 (2000).

⁹M. Balog, M. Schieber, M. Michman, and S. Patai, *Thin Solid Films* **41**, 247 (1977).

¹⁰G. D. Wilk, M. L. Green, M.-Y. Ho, B. W. Busch, T. W. Sorsch, F. P. Klemens, B. Brijis, R. B. van Dover, A. Kornblit, T. Gustafsson, E. Garfunkel, S. Hillenius, D. Monroe, P. Kalavade, and J. M. Hergenrother, *Tech. Dig. VLSI Symp.* **2002**, 88.

¹¹E. P. Gusev, D. A. Buchanan, E. Cartier, A. Kuman, D. DiMaria, S. Guha, A. Callegari, S. Zafar, P. C. Jamison, D. A. Neumayer, M. Copel, M. A. Gribelyuk, H. Okorn-Schmidt, C. D'Emic, P. Kozlowski, K. Chan, N. Bojarczuk, L.-Å. Ragnarsson, P. Ronsheim, K. Rim, R. J. Fleming, A. Mocuta, and A. Ajmera, *Tech. Dig. Int. Electron Devices Meet.* **2001**, 451.

¹²W. Zhu, T. P. Ma, T. Tamagawa, Y. Di, J. Kim, R. Carruthers, M. Gibson, and T. Furukawa, *Tech. Dig. Int. Electron Devices Meet.* **2001**, 464.

¹³J. M. Hergenrother, G. D. Wilk, T. Nigam, F. P. Klemens, D. Monroe, P. J. Silverman, T. W. Sorsch, B. Busch, M. L. Green, M. R. Baker, T. Boone, M. K. Bude, N. A. Ciampa, E. J. Ferry, A. T. Fiory, S. J. Hillenius, D. C. Jacobson, R. W. Johnson, P. Kalavade, R. C. Keller, C. A. King, A. Kornblit, H. W. Krautter, J. T.-C. Lee, W. M. Mansfield, J. F. Miner, M. D. Morris, S.-H. Oh, J. M. Rosamilia, B. J. Sapjeta, K. Short, K. Steiner, D. A. Muller, P. M. Voyles, J. L. Grazul, E. J. Shero, M. E. Givens, C. Pomarede, M. Mazanec, and C. Werkhoven, *Tech. Dig. Int. Electron Devices Meet.* **2001**, 51.

¹⁴A. Callegari, E. Cartier, M. Gribelyuk, H. F. Okorn-Schmidt, and T. Zabel, *J. Appl. Phys.* **90**, 6466 (2001).

¹⁵S. J. Lee, H. F. Luan, C. H. Lee, T. S. Jeon, W. P. Bai, Y. Senzaki, D. Roberts, and D. L. Kwong, *Tech. Dig. VLSI Symp.* **2001**, 133.

¹⁶M.-H. Cho, Y. S. Roh, C. N. Whang, K. Jeong, S. W. Nahm, D.-H. Ko, J. H. Lee, N. I. Lee, and K. Fujihara, *Appl. Phys. Lett.* **81**, 472 (2002).

¹⁷R. R. Manory, T. Mori, I. Shimizu, S. Miyake, and G. Kimmel, *J. Vac. Sci. Technol. A* **20**, 549 (2002).

¹⁸M. Gutowski, J. E. Jaffe, C.-L. Liu, M. Stoker, R. I. Hegde, R. S. Rai, and P. J. Tobin, *J. Appl. Phys.* **80**, 1897 (2002).

¹⁹M. Ritala and M. Leskelä, *Nanotechnology* **10**, 19 (1999).

²⁰M. Ritala, K. Kukli, A. Rahtu, P. I. Räisänen, M. Leskelä, T. Sajavaara, and J. Keinonen, *Science* **288**, 319 (2000).

²¹M. Leskelä and M. Ritala, *J. Phys. IV* **5**, 937 (1995).

²²P. M. Voyles, J. M. Gibson, and M. M. J. Treacy, *J. Electron Microsc.* **49**, 259 (2000).

²³T. Suntola, *Thin Solid Films* **216**, 84 (1992).

²⁴M. L. Green, M.-Y. Ho, B. W. Busch, G. D. Wilk, T. Sorsch, T. Conard, B. Brijis, W. Vandervorst, P. Räisänen, D. Muller, M. Bude, and J. Grazul, *J. Appl. Phys.* **92**, 7168 (2002).

²⁵R. Matero, A. Rahtu, M. Ritala, M. Leskelä, and T. Sajavaara, *Thin Solid Films* **368**, 1 (2000).

²⁶Brücker-AXS GmbH, Karlsruhe, Germany; <http://www.brucker-axs.com/production/indexie.htm>

²⁷R. B. van Dover, D. V. Lang, M. L. Green, and L. Manchanda, *J. Vac. Sci. Technol. A* **19**, 2779 (2001).

²⁸P. M. Voyles and D. A. Muller, *Ultramicroscopy* **93**, 147 (2002).

²⁹J. Aarik, A. Aidla, A.-A. Kiisler, T. Uustare, and V. Sammelselg, *Thin Solid Films* **340**, 110 (1999).

³⁰M. Ritala, M. Leskelä, L. Niinistö, T. Prohaska, G. Friedbacher, and M. Grasserbauer, *Thin Solid Films* **250**, 72 (1994).

³¹D. A. Muller, in *Characterization and Metrology for ULSI Technology: 2000 International Conference*, edited by D. G. Seiler, A. C. Diebold, T. J. Shaffner, R. McDonald, W. M. Bullis, P. J. Smith, and E. M. Secula (AIP, New York, 2001), p. 500.

³²B. W. Busch, I. Pluchery, Y. J. Chabal, D. A. Muller, R. L. Opila, J. R. Kwo, and E. Garfunkel, *MRS Bull.* **27**, 206 (2002).

³³P. S. Lysaght, P. J. Chen, R. Bergmann, T. Messina, R. W. Murto, and H. R. Huff, *J. Non-Cryst. Solids* **303**, 54 (2002).